André Orth*, Hawo H. Höfer, Leonie Wildersinn, Fabian Jeschull, and Markus Reischl

ML-Driven Contamination Classification for XPS Analysis of PLA Surfaces

https://doi.org/10.1515/cdbme-2025-0184

Abstract: As materials such as Poly-Lactic Acid (PLA) have become a significant part of medical production and research, it is important that the resulting products adhere to strict regulations concerning contaminations. A wide variety of methods are currently used to comply with these regulations depending on the products and their intended use case.

We propose a standardized workflow for high-sensitivity contamination detection in X-ray photoelectron spectroscopy (XPS) survey scans that helps enhance detection reliability, reduce throughput constraints associated with manual analysis and streamline an automated analysis. This makes XPS a more viable option for process monitoring and reduces the need for additional analysis steps.

The workflow uses a neural network trained on synthetic signals to predict contamination at%. These are then compared with individually variable contamination limits to classify each contaminant.

Keywords: XPS, X-ray Photo Electron Spectroscopy, Contamination Detection, Machine Learning, Synthetic Dataset

1 Introduction

Poly-Lactic Acid (PLA) is a biodegradable polymer that has a multitude of medical applications due to its biocompatibility, biodegradability, and versatility. Common use cases are implants and drug delivery systems. For such applications it is important to reduce risks of contamination to prevent inflammatory responses, degradation or allergic reactions [1–3].

The detection is highly dependent on instruments used, needed depth of detection, destructive or non-destructive analysis, amount of measurements and necessary accuracy. Existing methods use Fourier Transform Infrared Spectroscopy (FTIR), Raman Spectroscopy, Pyrolysis-Gas Chromatography-Mass Spectrometry (Py-GC/MS) and X-ray Photoelectron Spectroscopy (XPS).

*Corresponding author: André Orth, Institute for Automation and Applied Informatics, Karlsruhe Institute of Technology (KIT), Eggenstein-Leopoldshafen, Germany, e-mail: andre.orth@kit.edu Hawo H. Höfer, Markus Reischl, Institute for Automation and Applied Informatics, KIT, Eggenstein-Leopoldshafen, Germany Leonie Wildersinn, Fabian Jeschull, Institute for Applied Materials Energy Storage Systems, KIT, Eggenstein-Leopoldshafen, Germany

Unlike FTIR and Raman, XPS provides nanoscale surface sensitivity (≤10 nm depth), enabling direct detection of contaminants critical to medical device biocompatibility [4, 5].

Furthermore, XPS is vital for batch testing in pharmaceutical packaging as survey scans (200 eV pass energy) achieve full elemental inventories in <10 minutes. FTIR and Raman require further deconvolution to distinguish overlapping organic bands and Py-GC/MS is limited to volatile organics [6, 7].

Finally, non-destructiveness is critical for implantable devices requiring multifactorial validation. FTIR, Raman, and XPS fit this requirement, offering complementary insights. While FTIR and Raman provide molecular fingerprinting across the sample, XPS delivers precise elemental analysis of the outermost 10 nm surface - critical for biocompatibility. Though Py-GC/MS requires pyrolysis (destroying μ g-scale samples), this is often acceptable for quality assessment. Its limitation lies in detecting only volatile thermal decomposition products [5, 7].

We therefore have chosen XPS as our contamination detection method due to its unparalleled surface sensitivity and quantitative elemental identification capabilities, critical for detecting trace contaminants in medical devices [8, 9]. However, traditional XPS analysis is inherently time-consuming, as it depends on manual peak fitting and interpretation. This requires trained experts and can become error-prone as well as limit throughput for large-scale quality control [10, 11].

To address these limitations, we propose an ML-driven workflow combining regression models for atomic percentage (at%) prediction with contamination threshold classification, enabling automated high-sensitivity survey scan analysis. Our approach improves detection reliability while addressing the significant throughput limits of ~ 10 samples/day via manual XPS vs. 100+ via automated FTIR/Raman. By enabling real-time analysis of thousands of XPS signals, we bridge this gap while preserving XPS's surface specificity, particularly for halogenated contaminants critical to PLA's biocompatibility and degradation in medical applications.

2 Method

As exemplary contaminants, we have chosen chloride (Cl⁻), which may originate from saline rinsing or bleach residues, fluorine (F) potentially leaching from equipment made of poly(vinylidene difluoride) (PVDF) and silicon (Si) from silicone mold release agents. These can be substituted with others depending on the manufacturing context. The necessary data for training and testing is generated synthetically, as freely available XPS measurements are not sufficiently available.

The application of the workflow is shown in Figure 1. After manufacturing or handling of the PLA-based product, an XPS survey scan is done. A trained neural network then predicts an at% for each contaminant. Based on these values a subsequent classification can be executed using a contamination limit. Here, the limit is set to 0.1 at%, which according to Lefebvre et al. [12] is the general order of the elemental sensitivity of XPS.

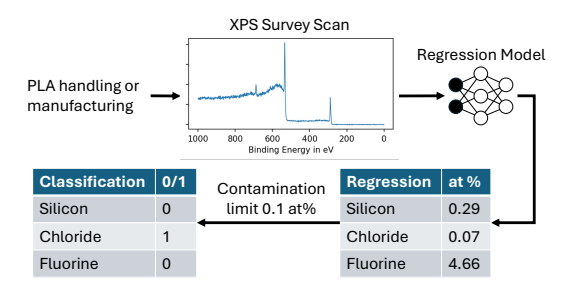


Fig. 1: Workflow of the contamination detection

To predict contaminants as an output of the neural network, we first need synthetic input signals to train the neural network. The data pipeline to generate synthetic survey signals is based on our previous work which was focused on XPS detail scans [13]. The previously used background method is replaced to accommodate survey signals with a wider range of binding energies. Additional parameters as in width and noise type are adjusted for the generation of realistic survey signals. An illustrated overview of the updated data pipeline is shown in Figure 2. It consists of three main steps: Generation of 'pure peaks', a 'background' and a final addition of 'noise' to create a synthetic survey signal.

As first step, we generate a signal that consists of 'pure peaks' for each chemical state (brown signal in Figure 2). To accomplish this, we first define peak parameters and sample at% labels for contaminants and PLA. These labels are converted into peak areas, which are then used to generate and combine individual peaks, reconstructing the synthetic spectrum.

In Table 1, the chemical states of all involved elements as well as their peak center binding energies (BE), peak width ranges (Full Width Half Maximum, FWHM) and Relative Sensitivity Factors (RSF) are listed. The chosen FWHM ranges are broader than usual detail scan ranges. This is based on the use of higher pass energies during survey scans to maximize

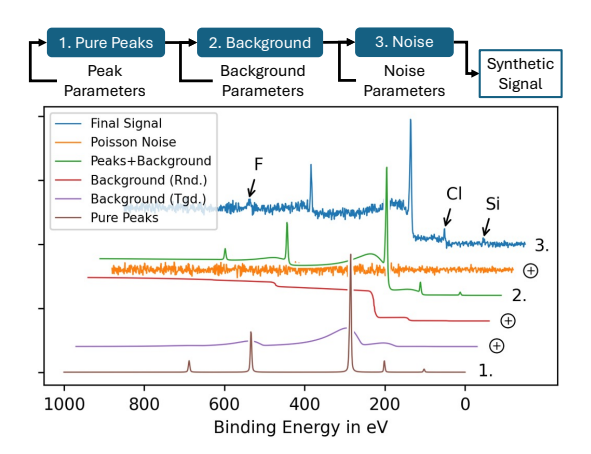


Fig. 2: Pipeline for the generation of synthetic survey signals

throughput across a wide binding energy range which results in broader peaks.

Tab. 1: Peak parameters for chemical states of contaminants and PLA

Chemical state	BE /eV	FWHM /eV	RSF
C 1s (C-C, C-H)	285.0	2.5-4.0	1
C 1s (C-O)	286.8	2.5-4.0	1
C 1s (C=O)	288.8	2.5-4.0	1
O 1s (C=O)	531.8	3.0-4.5	2.93
O 1s (C-O)	533.6	3.0-4.5	2.93
Si 2p (Si-C)	101.8	2.5-4.0	0.817
Si 2p (Si-O)	103.5	2.5-4.0	0.817
Cl ⁻ 2p3/2	198.7	2.5-4.0	2.29
Cl ⁻ 2p1/2	200.3	2.5-4.0	2.29
F1s	688.0	3.0-4.5	4.43

We keep the possible at% for each contaminant within a reduced range of [0, 5]. This limits the scope to residues, reduces training with unnecessary data and can be adapted to specific use cases. Therefore, the base at% labels for the contaminants (Si, Cl⁻, F) are each uniformly sampled from a range of [0.0, 5.0]. Si and Cl⁻ with more than one chemical state are split by multiplying them with another uniformly sampled array (range [0.0, 1.0]) to allocate varying shares to each state.

Afterwards, the PLA chemical states are uniformly sampled from [0.0, 1.0] and normalized to the remaining at% not occupied by contaminants. From these final atomic shares, we then calculate the peak area shares using the given RSF from Table 1 by dividing each atomic share with the respective RSF. The additional peak parameters are uniformly sampled from the given ranges of Table 1.

Now, for each chemical state a pseudo-Voigt peak is created with the FWHM, normalized to an area of 1 and multiplied with its peak area share. Adding all 'pure peaks' together

gives the base signal. This is repeated for the required amount of synthetic signals. In Figure 3 three different contamination levels are displayed with equal parts for all contaminants.

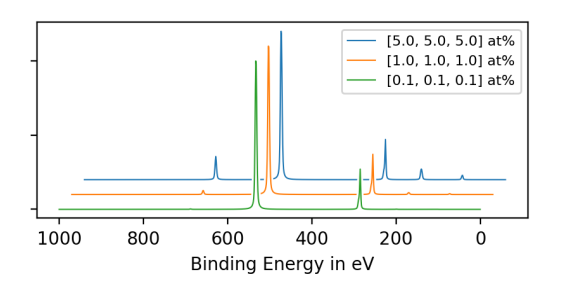


Fig. 3: Comparison of peaks at different contamination levels

Next, we address background generation as second step in our data pipeline (Figure 2). While the pseudo-Shirley method used in [13] was sufficient for generating basic detail scan backgrounds, we want to account for more complex effects. Therefore, we generate a multitude of backgrounds based on different functions to train the network to focus on contaminant peak areas in relation to PLA. This method uses a Tougaard ('Tgd.', purple) and variable ('Var.', red) component. Both components require parameters that are sampled within predefined ranges to generate realistic backgrounds.

The 'Tgd.' component is based on the Tougaard method [14], which is used to subtract backgrounds with high amounts of inelastic scattering. It is an iterative method that uses an inelastic electron scattering cross-section K for which the 2-parameter approach in Equation 1 is mostly used. The parameters B and C shape the calculated background depending on material parameters and previous know-how.

$$K(x) = \frac{Bx}{(C+x^2)^2}$$
 (1)

In our modified Tougaard approach, we sample B and C with interdependent values that are larger than typical, reflecting the specific requirements of our use case, before scaling the resulting component.

The additional variable component 'Var.' is added to account for more than the shape of an immediate scattering background. For each peak, a shape is randomly chosen from the base trail types ('linear', 'quadratic', 'exponential' and 'mixed'). These types define the general function of the background component for each single peak to emulate the shapes in Tougaard et al. [15] based on different surface concentration distributions. The functions use a sampled gradient parameter for a general trend and an additional scaling parameter.

The two background components are then combined, smoothed with a Gaussian filter to generate the final backgrounds for our survey signals, and added to the 'pure peaks'. For the final step in Figure 2 (orange and blue signal), the base signals are normalized to [0, 1] and Poisson noise is added. As Poisson noise calculation depends on the supplied signal values and its gradients, it is temporarily scaled and offset to generate different amounts of noise.¹

Following dataset generation, we train a CNN-based regression model on synthetic signals to predict at% for each contaminant. The predicted at% are then evaluated against predefined contamination limits to classify contamination events.

The model uses three 1D convolutional layers (Conv1D) with increasing filter counts (16, 32, 48), kernel size of 9 and ReLu activation to extract features from the XPS signal. Each Conv1D is followed by a max-pooling layer to reduce dimensionality. After flattening the output from the Conv1D, a dense layer with 128 neurons processes these features. The output layer has 3 neurons with ReLu activation functions, producing independent probability values for each contaminant.

Root Mean Squared Error (RMSE) was chosen as loss to train the model. We utilize Adam with a base learning rate of $1e^{-4}$ as optimizer and adjusted with the Keras class 'ReduceLROnPlateau'. To prevent unnecessary training epochs, Keras' EarlyStopping feature was applied. For result comparison, RMSE and standard deviations of each contaminant prediction are used as well as subsequently calculated accuracies based on the contamination limit of 0.1 at%.

3 Results

For the final results, the data pipeline was used to create 2,000,000 synthetic signals within 40 minutes. The data is split into two parts of 80 % training and 20 % testing, of which the training part is further split (80 % for actual training, 20 % for validation). The training of the model took 23 minutes on an NVIDIA RTX 3090 Ti and was stopped after 80 epochs.

The overall achieved RMSE is 0.003 with a standard deviation of (0.00179, 0.00173, 0.00283) for each contaminant (Si, Cl⁻, F). Converting the regression predictions to binary values with the contamination limit at 0.1 at% for each contaminant, the overall accuracy scores 98.34 %.

Figure 4 shows the prediction error of the model in a histogram. From this can be derived that 98.71 % of the predictions have an error below 1 at%, 91.72 % below 0.5 at% and still 37.38 % remain below the elemental sensitivity of XPS at 0.1 at%. Comparing predictions with the highest (blue) and lowest error (orange) in Figure 5 shows the highest predic-

¹ Offset values from a range of [1, 100] and multipliers from [250, 5000] are sampled. Higher offsets generate higher and more uniform noise across the signal while lower multipliers generate stronger noise around peaks.

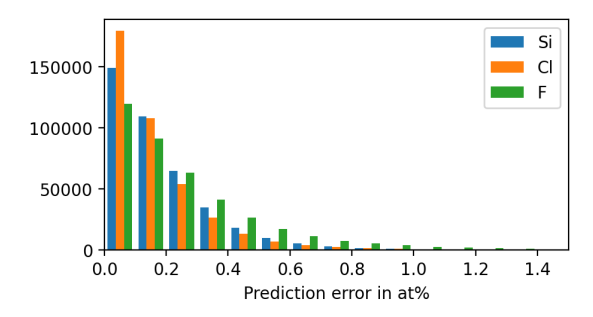


Fig. 4: Histogram of prediction error (abs(true - predicted) at%)

tion error for the prediction with a lower signal-to-noise ratio (SNR). This is a general trend as the more extreme Poisson noise can partially mask contamination peaks. As survey scans tend to have higher SNR, this benefits our prediction accuracy.

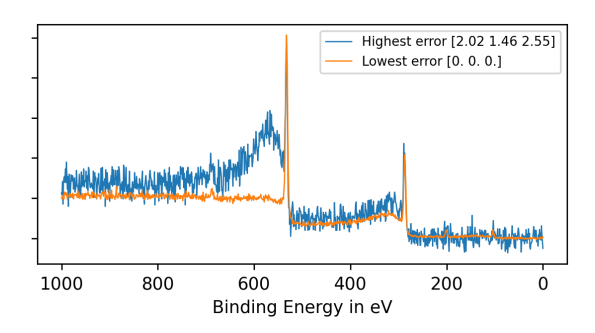


Fig. 5: Comparison of best and worst prediction

4 Conclusion

Standardizing contamination detection for medical materials like PLA using XPS survey scans and accelerating throughput is an important task. The findings of Baer et al. [10] with only 40 % of XPS signals classified as 'minor' or 'no issues' show the urgent need for robust assistive solutions. Our workflow addresses this by enabling high-throughput XPS-based contamination detection, achieving 98.34 % classification accuracy for multiple contaminants. By combining XPS's surface-specific elemental precision with automated, consistent impurity detection, we establish a practical solution for medical manufacturing quality control where trace contaminants directly impact PLA biocompatibility.

While these results are demonstrated in a limited scope, next steps include validation on real-world data and incorporation of e.g. compound ratio constraints. The method's modular design allows extension to other materials and extension with detail scan analysis from our prior work.

References

- D. da Silva et al. "Biocompatibility, biodegradation and excretion of polylactic acid (PLA) in medical implants and theranostic systems." In: *Chemical engineering journal* 340 (2018), pp. 9–14.
- [2] M. A. Cuiffo et al. "Impact of the Fused Deposition (FDM) Printing Process on Polylactic Acid (PLA) Chemistry and Structure." In: Applied Sciences 7.6 (2017), p. 579.
- [3] Z. Yang et al. "Medical applications and prospects of polylactic acid materials." In: iScience 27.12 (2024), p. 111512.
- [4] I. D. Morais et al. "Preventing Candida albicans Contamination on Packaged Ti-6Al-4V Alloy Surfaces by Cold Atmospheric Plasma Treatment." In: ACS Applied Bio Materials 8.3 (2025), pp. 1956–1962.
- [5] A. López-Camacho et al. "Study of the bactericidal properties of polylactic acid-based 3D filament." In: *Journal of Vinyl and Additive Technology* (2025), vnl.22216.
- [6] B. J. Kulbacki et al. "Analysis of silver metal with a Thermo Scientific K-Alpha XPS instrument at 50 and 200 eV pass energies." In: Surface Science Spectra 31.2 (2024), p. 024005.
- K. M. Cole et al. "Co3O4 nanoparticles characterized by XPS and UPS." In: Surface Science Spectra 28.1 (2021), p. 014001.
- [8] S. V. Bhujbal et al. "Qualitative and Quantitative Characterization of Composition Heterogeneity on the Surface of Spray Dried Amorphous Solid Dispersion Particles by an Advanced Surface Analysis Platform with High Surface Sensitivity and Superior Spatial Resolution." In: Molecular Pharmaceutics 15.5 (2018), pp. 2045–2053.
- [9] T. Eickner et al. "XPS-Analysis of solvent residues in different polymeric biomaterials." In: *Current Directions in Biomedical Engineering* 8.2 (2022), pp. 584–587.
- [10] D. R. Baer et al. "Evolving efforts to maintain and improve XPS analysis quality in an era of increasingly diverse uses and users." In: Surface and Interface Analysis 55.6-7 (2023), pp. 480–488.
- [11] M. Bruggeman et al. "Processing and interpretation of core-electron XPS spectra of complex plasma-treated polyethylene-based surfaces using a theoretical peak model." In: Surface and Interface Analysis 54.9 (2022), pp. 986–1007.
- [12] J. Lefebvre et al. "Experimental methods in chemical engineering: X-ray photoelectron spectroscopy-XPS." In: *The Canadian Journal of Chemical Engineering* 97.10 (2019), pp. 2588–2593.
- [13] A. Orth et al. "ML-Based XPS Quantification Supported by Synthetic Dataset Generation." In: Current Directions in Biomedical Engineering 10.4 (2024), pp. 482–485.
- [14] S. Tougaard. "Quantitative analysis of the inelastic background in surface electron spectroscopy." In: *Surface and Interface Analysis* 11.9 (1988), pp. 453–472.
- [15] S. Tougaard. "Practical guide to the use of backgrounds in quantitative XPS." In: *Journal of Vacuum Science & Technology A* 39.1 (2020), p. 011201.